Article

Design and Experimental Verification of Pressurized Cylinders in Hydraulic Rubber Hose Pressure Washers

Xiaoxiao Niu [1], Guangfa Hao [1], Chengliang Zhang [1,*] and Lei Li [2]

[1] School of Mechanical Engineering, University of Jinan, Jinan 250022, China; 202021100292@mail.ujn.edu.cn (X.N.); 201821200564@mail.ujn.edu.cn (G.H.)

[2] School of Mechanical and Automotive Engineering, Qilu University of Technology (Shandong Academy of Sciences), Jinan 250353, China; lilei9lily@163.com

* Correspondence: me_zhangcl@ujn.edu.cn

Abstract: Hydraulic rubber hoses are subject to great hydraulic impact during the actual working process, which causes a great potential safety hazard. Therefore, it is necessary to carry out pressure tests on hose assemblies to ensure its quality, so providing a high pressure for the hydraulic hose has become the key technology of this problem. Aiming at solving the problem of detection of pressure resistance in hydraulic rubber hose cleaning machines, this paper analyzed the pressurization mechanism of the hydraulic pressurized cylinder and proposed a method of continuous pressurization. This paper also theoretically analyzed the pressure expansion of the rubber hose, and the conclusion is that for the maximum hose capacity (hose size is $\Phi 25$ mm $\times$ 6 m), the volume of water required to provide water in the hose from 10 MPa to 100 MPa is 0.59 L. The pressurized cylinder was designed and checked theoretically and analyzed by the finite element method. It is concluded that the maximum stress of the pressurized cylinder is concentrated at the bottom of the high-pressure chamber, and the outlet hole at the bottom of the cylinder barrel of the high-pressure chamber is the weakest part of the pressurized cylinder. The performance of the supercharging cylinder is verified by experiments, which proves the feasibility, rapidity and stability of the supercharging cylinder.

Keywords: hydraulic rubber hose; double-acting pressurized cylinder; pressure test; compression expansion; finite element

1. Introduction

Hydraulic hose assemblies are widely used in various types of hydraulic equipment, especially in heavy-duty hydraulic equipment such as excavators, loaders and bulldozers [1,2]. In the actual work process, it is often affected by high and low temperature changes outside. Due to the harsh construction environment, they will be subject to great hydraulic impact, it is very likely that there will be hydraulic oil leakage, buckle tripping, hose bursts and other situations, which will cause great security risks and endanger the safety of people and machines [3–5]. In order to solve these problems, it is necessary to carry out pressure tests on the hose assemblies to ensure their quality, so providing high pressure for the hydraulic hose has become the key technology of this problem [6,7].

At present, gas-liquid booster pumps are used in the pressure test bench [8,9], but their pressure loading is unstable and the fluctuations are difficult to control [10]. The flow rate is only 0.3 L/min, and the pressurization takes a long time. They can only complete the pressure test of 2 m of rubber hose assembly at a time, so it takes a long time to complete the pressure test of a large number of rubber hoses, which cannot meet requirements of the production line, therefore, it is urgent to adopt a new pressurization method to improve the pressure test efficiency of rubber hose assemblies [11–13].

In normal engineering applications, the pressure of general hydraulic systems is within 35 MPa. Under this pressure condition, the cost and maintenance cost of the hydraulic system are relatively low, so it has high economic benefits. But in some cases

such as metal extrusion, ultra-high pressure water jet processing, hydroforming, pressure explosion testing and so on, the pressure is usually about 100 MPa, and sometimes even higher. When the pressure of a hydraulic system exceeds 82 MPa, it can be considered as an ultra-high pressure system, and its cost and maintenance cost are considerable [14,15]. It is difficult for a typical high-pressure pump to achieve such a high pressure, so a pressurized cylinder is usually used to achieve the desired pressure [16,17].

In order to solve the above problems, this paper adopts a liquid-driven double-acting pressurized cylinder which uses oil pressure to increase the water pressure, so as to provide high water pressure for the withstand voltage test. A booster circuit is set in the low pressure chamber of the double-acting pressurized cylinder, the pressure of the circuit is adjustable, and hydraulic oil functions as the medium to achieve the purpose of system supercharging; a theoretical analysis and calculation of the compression expansion of the hose are carried out, and the key dimensions of the pressurized cylinder are designed and calculated according to the calculation results. The strength of the hydraulic cylinder is checked and finite element simulation is carried out under different working conditions. The theoretical calculation results are compared with the simulation results, and the performance of the hydraulic cylinder is verified by experiments.

As the pressure and cleanliness of the hydraulic system have higher and higher requirements on the hoseline, it is urgent to adopt new process plans and equipment to ensure the cleanliness of the hoseline and to detect the pressure resistance of the hoseline. This study can improve the efficiency and stability of hose cleaning and promote the improvement of production efficiency. The cleaning, pressure testing and drying integrated process equipment of hose has good application prospects, which can promote the development of the hose industry.

2. Hydraulic Cylinder Pressure Ratio Theoretical Calculation

In this paper, the double-acting pressurized cylinder is adopted, which is in the form of a double-extraction rod [18–20]. There is no idle stroke, which improves the working efficiency. The low-pressure chamber is an oil chamber, the inner diameter is d; the high pressure chamber is a water chamber, and the inner diameter is D [21]. The two high pressure water chambers are connected to a circuit consisting of four check valves. When the pressurized cylinder piston moves to the left, the left chamber discharges high pressure water and the right chamber suctions in water. When the piston moves to the right, the right chamber discharges high pressure water and the left chamber suctions in water. The water suction and discharge processes are simultaneously performed, and the input lower pressure hydraulic oil is converted into higher pressure water for use in the hose pressure test system. A structure diagram is shown in Figure 1.
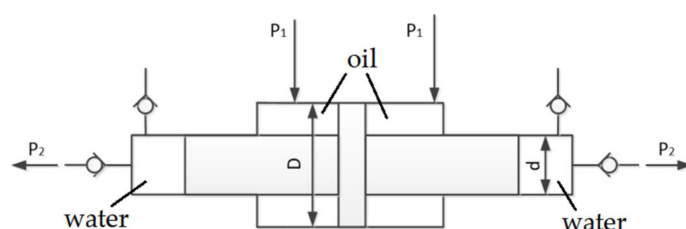

Figure 1. Schematic diagram of double-acting pressurized cylinder.

In Figure 1, the input pressure of the low-pressure chamber of the pressurized cylinder is P_1, and the output pressure of the high pressure chamber is P_2. The mechanical balance is obtained without considering the resistance:

$$\frac{\pi}{4}\left(D^2 - d^2\right)P_1 = \frac{\pi}{4}d^2 P_2 \tag{1}$$

$$\frac{D^2 - d^2}{d^2} = \frac{P_1}{P_2} \tag{2}$$

where $\frac{D^2}{d^2}$ is the boost ratio.

3. Pressurized Cylinder Flow Demand Calculation

3.1. Selection of Pressurized Medium and Determination of Technical Indicators

The system pressure during pressure test is very high. The ultra-high pressure system requires the hydraulic medium to have good flowability and small volume compression. However, water has high bulk modulus of elasticity, so it is suitable to be used as hydraulic medium in the proposed pressure test system.

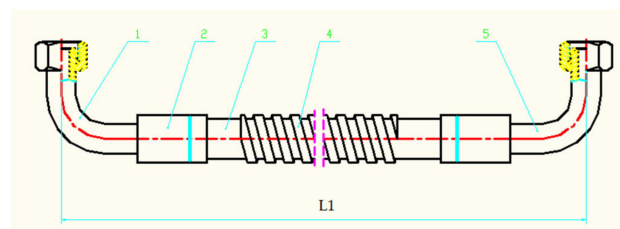The structure of hydraulic hose assembly is shown in Figure 2.

Figure 2. Hydraulic hose assembly. 1—connector 1; 2—sleeve; 3—hose; 4—spring sheath; 5—connector 2.

The pressurized cylinder provides a pressure source for the pressure test of the hydraulic hose. The pressure test requires that the hydraulic hose of the type 12EFG6K will be pressurized to 100 MPa within the specified time. The details of the hose are shown in Table 1. For this hose, it is considered that the total amount of compression caused by water pressure and the total deformation produced by the compression of hose assembly are the demands of the supercharging system in terms of flow rate, while the deformation produced by the rigid hose loop is ignored. In summary, the system pressure requirement is 100 MPa, and the maximum capacity of the hydraulic hose assembly to be tested is 6000 mm in length and Φ25 mm in diameter.

Table 1. Hose parameter.

Content	Numerical Value
brand	GATES
type	12EFG6K
diameter	25 mm
length	6000 mm

3.2. Calculation of the Amount of Compression Generated by Water Compression

The maximum volume V_1 of the test hose assembly is:

$$V_1 = \frac{\pi d_1^2 L_1}{4} \tag{3}$$

where d_1 is the diameter (mm) of the test hose assembly; L_1 is the total length (mm) of the test hose assembly.

At room temperature, water compression coefficient β_w is $4.5 \times 10^{-4} \left(MPa^{-1} \right)$, and the test bench pre-fills the hose before the test of the hose. The pressure of the pre-filling liquid is 10 MPa. When the pressure is increased from 10 MPa to 100 MPa, the compression amount ΔV_1 generated by the water pressure is:

$$\Delta V_1 = V_1 \Delta P \beta_w = V_1 (P - P_0) \beta_w \tag{4}$$

where P is the pressure after water is pressurized; P_0 is the pressure of pre-flush before water is pressurized; β_w is water's compression coefficient.

3.3. Volume Change Calculation Caused by the Deformation of the Hose Assembly

Xu in his master's thesis [22] carried out a finite element analysis and simulation on the skeleton structure of a steel wire wound hydraulic hose. In this paper, the relevant conclusions of the change of the axial deformation of the hose body during the pressure application and the change of the radial deformation of the hose body during the pressure application are directly cited as the calculation basis. The conclusion of the paper points out that the deformation of the Φ25 mm diameter steel wire wrapped with the pressure varies with the pressure. The axial deformation of the Φ25 mm diameter is very slow. When the pressure is greater than 15 MPa, the axial deformation of the hose changes linearly. The amount of change in the inner diameter of the hose gradually increases as the applied pressure increases, and changes substantially linearly [22].

The hose with the model of 16M3K and 210 mm is selected for pressure test on the pressure tester. The diameter of the hose is Φ25 mm, and the working pressure is 27.6 MPa. Therefore, according to the 1.5 times working pressure factor, the maximum pressure can be increased to 40 MPa, and the axial deformation and radial deformation are recorded at 5 MPa per liter. The experimental data is processed. Figure 3 shows the change of the axial deformation of the hose with the pressure process. Figure 4 shows the change of the inner diameter of the hose with the pressure process [22].
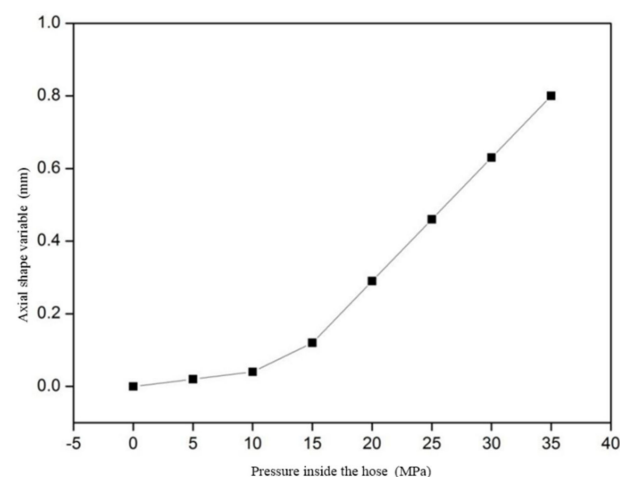

Figure 3. Variation of the axial deformation of the hose with the pressure application process.
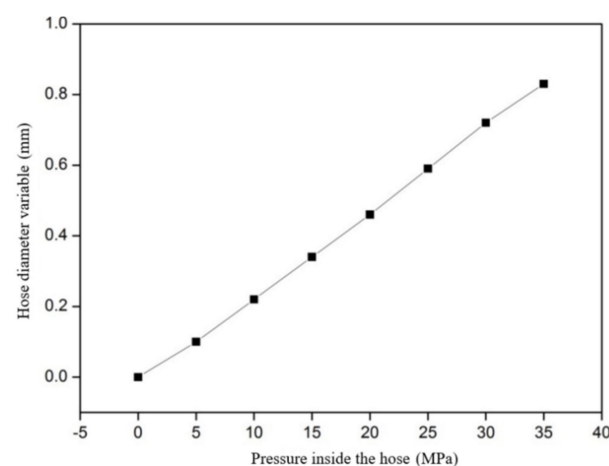

Figure 4. Variation of the inner diameter of the hose with the pressure application process.

It can be seen from Figure 3 that the axial deformation is 0.03 mm when the pressure is 10 MPa, and the axial length deformation of the hydraulic hose under pressure is −0.014%. In Figure 3, the axial deformation is 2.82 mm when the pressure is 100 MPa. Therefore, the axial length deformation of the hydraulic hose under pressure is −1.34%. It meets the mechanical industry standard JB/T8727-2004 which stipulates that the axial length deformation of the hose under pressure is −2–4%. When the length of the hose assembly is 6000 mm, the length becomes 5999.1 mm after being subjected to a pressure of 10 MPa, and the length becomes 5919.6 mm after being subjected to a pressure of 100 MPa.

As Figure 4 illustrates, when the pressure is 10 MPa, the inner diameter deformation is 0.2 mm, and the hose diameter becomes Φ25.2 mm. For Figure 4, it can be estimated that when the pressure is 100 MPa, the inner diameter deformation is 2.34 mm and the hose diameter is changed to Φ27.3 mm. The ΔV_2 of the volume change caused by the deformation of the hose assembly is:

$$\Delta V_2 = \frac{\pi}{4}\left(d_n^2 L - d_0^2 L_0\right) \tag{5}$$

where d_n is the diameter (mm) of the hose when subjected to a pressure of 100 MPa; d_0 is the diameter (mm) of the hose when subjected to a pressure of 10 MPa; L is the total length (mm) of the hose when subjected to a pressure of 100 MPa; L_0 is the total length (mm) of the hose when subjected to a pressure of 10 MPa.

3.4. Calculation of Volume Change of Pressurized System

The total volume change ΔV is:

$$\Delta V = \Delta V_1 + \Delta V_2 \tag{6}$$

Substituting the relevant data into the above theoretical formula, it can be analyzed that for the hydraulic hose of the type 12EFG6K, the capacity of supplying water to the hose is 0.59 L from 10 MPa to 100 MPa.

4. Design Calculation and Strength Check of the Pressurized Cylinder
4.1. Design and Calculation of Double-Acting Liquid Drive Pressurized Cylinder

Through the analysis of the pressurization theory of the hydraulic hose, we got the working requirement of adding the cylinder: for the hydraulic hose of the type 12EFG6K, the pressure increases from 10 MPa to 100 MPa within the specified time, and the required water supply capacity to the hose is 0.59 L. According to the above conclusions, this paper presents the relevant parameters of the pressurized cylinder to design and calculate. The preset parameters of the pressurized cylinder are shown in Table 2.

Table 2. Pre-set parameters of the pressurized cylinder.

Pre-Set Content	Numerical Value
inner diameter of high pressure cavity (mm)	45
number of piston runs	3
boost ratio	1:7
pressure of high pressure cavity (MPa)	100
pressure of low pressure cavity (MPa)	10

The formula for calculating the total stroke L_z of the pressurized cylinder is:

$$L_z = \frac{\Delta V}{\frac{\pi d^2}{4}} \tag{7}$$

The formula for calculating the single stroke L_r of the pressurized cylinder is:

$$L_r = \frac{L_z}{6} \tag{8}$$

The relevant data is substituted into the formula to solve the actual design parameters of the pressurized cylinder, as shown in Table 3.

Table 3. Actual design parameters of the pressurized cylinder.

Actual Content	Numerical Value
single stroke (mm)	65
inner diameter of low pressure cavity (mm)	130
inner diameter of high pressure cavity (mm)	45
boost ratio	1:7.3
pressure of low pressure cavity (MPa)	13.7
pressure of high pressure cavity (MPa)	100

According to the above conditions, we have designed a double-acting pressurized cylinder [23,24]. The assembled diagram of the designed pressurized cylinder is shown in Figure 5, where the oil chamber 8 and the water chamber 12 constitute two chambers of the pressurized cylinder. The seal between the piston 2 and the low-pressure chamber cylinder 6 is made of a grate ring with a working pressure of 40 MPa [25], which is much higher than the low pressure. The required oil pressure in the chamber is 13.7 MPa, which meets the working requirements. The seal between the piston 2 and the high pressure chamber cylinder 1 is sealed by a U-shaped slip ring type [26], and its maximum withstand voltage can reach 300 MPa, which is much larger than the water pressure of up to 100 MPa in the high pressure chamber to meet the working requirements. The static seal between the low-pressure cavity cylinder 6 and the high-pressure cavity cylinder 1 is sealed by an O-ring [27]. The working pressure can reach 40 MPa, which is much larger than 13.7 MPa, so it satisfies the working requirements. A ring 4 is provided in the high- pressure chamber to cushion the piston 2 [28].
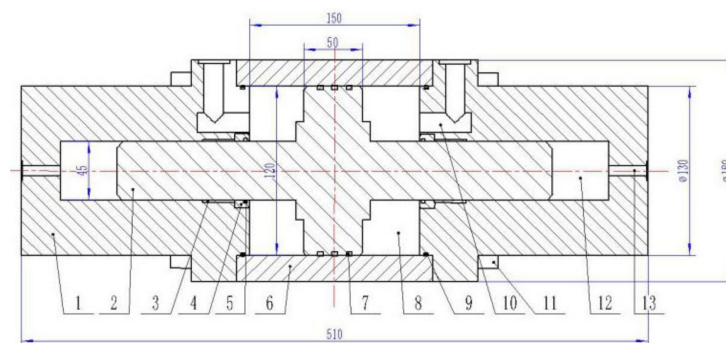

Figure 5. Assembly drawing of the pressurized cylinder. 1—high pressure chamber cylinder; 2—piston rod; 3—support ring; 4—block; 5—u-slip ring combination seal; 6—low pressure chamber cylinder; 7—hole with glyph ring; 8—oil chamber; 9—O seal; 10—inlet port; 11—hex socket head bolt; 12—water chamber; 13—outlet.

4.2. Double-Acting Liquid-Drive Pressurized Cylinder Strength Theory Check

The material used in this pressurized cylinder is 45# steel, which is a steel material with a tensile strength of $\sigma_b \geq 600$ MPa and a yield strength of $\sigma_s \geq 335$ MPa. For steel materials, the third or fourth strength theory in material mechanics is generally used. However, the third strength theory only considers the maximum shear stress, while the von Mises theory considers the combined effects of the three principal stresses. Therefore, this paper uses the von Mises theory for strength checking.

4.2.1. Cylinder Strength Check Calculation

Figure 6 [29] shows the physical stress distribution of the micro-body in the three-dimensional stress state of the thick-walled cylinder.
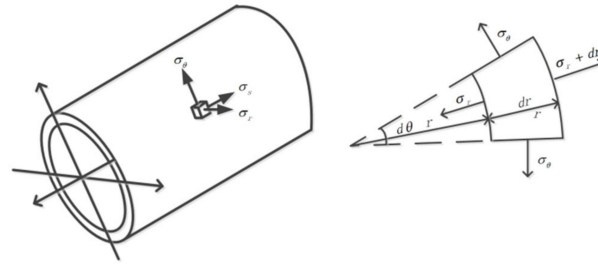

Figure 6. Stress distribution of the micro-body of a thick-walled cylinder.

The distribution law of the three-direction stress is obtained from the theoretical calculation formula of thick-walled cylinder:

$$\begin{cases} \sigma_r = \dfrac{PR_i^2}{R_0^2 - R_i^2}\left(1 - \dfrac{R_0^2}{r^2}\right) = \dfrac{P}{K^2 - 1}\left(1 - \dfrac{R_0^2}{r^2}\right) \\[2ex] \sigma_\theta = \dfrac{PR_i^2}{R_0^2 - R_i^2}\left(1 + \dfrac{R_0^2}{r^2}\right) = \dfrac{P}{K^2 - 1}\left(1 + \dfrac{R_0^2}{r^2}\right) \\[2ex] \sigma_s = \dfrac{PR_i^2}{R_0^2 - R_i^2} = \dfrac{P}{K^2 - 1} \end{cases} \tag{9}$$

where σ_r is radial compressive stress, which is generated by the direct acting of the pressure oil on the inner wall of the cylinder wall; σ_θ is tangential tensile stress, which is caused by the radial expansion of the cylinder wall by internal pressure; σ_s is axial tensile stress, which is generated when pressure oil acts on both ends of the working chamber of the cylinder; P is test pressure; R_0 is the outer wall radius of the cylinder; R_i is the radius of the inner wall of the cylinder; r is free radius of the cylinder $(R_i \leq r \leq R_0)$; K is the ratio of R_0 to R_i.

The von Mises theory is:

$$[\sigma] = \sqrt{\frac{1}{2}\left[(\sigma_r - \sigma_\theta)^2 + (\sigma_\theta - \sigma_s)^2 + (\sigma_s - \sigma_r)^2\right]} \tag{10}$$

We substitute the above three-direction stress Formula (9) into (10). when $r = R_i$, the total stress is the largest, and the result is:

$$[\sigma] = \sqrt{3}\,\frac{PK^2}{K^2 - 1} \tag{11}$$

According to the above formula and the size of the pressurized cylinder designed in the previous section, the calculation formula of safety factor n_G is:

$$n_G = \frac{\sigma_b}{[\sigma]} \tag{12}$$

Substituting the relevant data into the formula can obtain the relevant parameters of the boost cylinder, as shown in Table 4. From the calculation results in Table 4, we can get the cylinder of the pressurized cylinder to meet the strength requirements.

Table 4. Pressurized cylinder stress parameters.

Cylinder's Name	Maximum Stress (MPa)	Safety Factor	Tensile Strength (MPa)
high pressure cylinder	220.65	2.71	600
low pressure cylinder	50.12	11.97	600

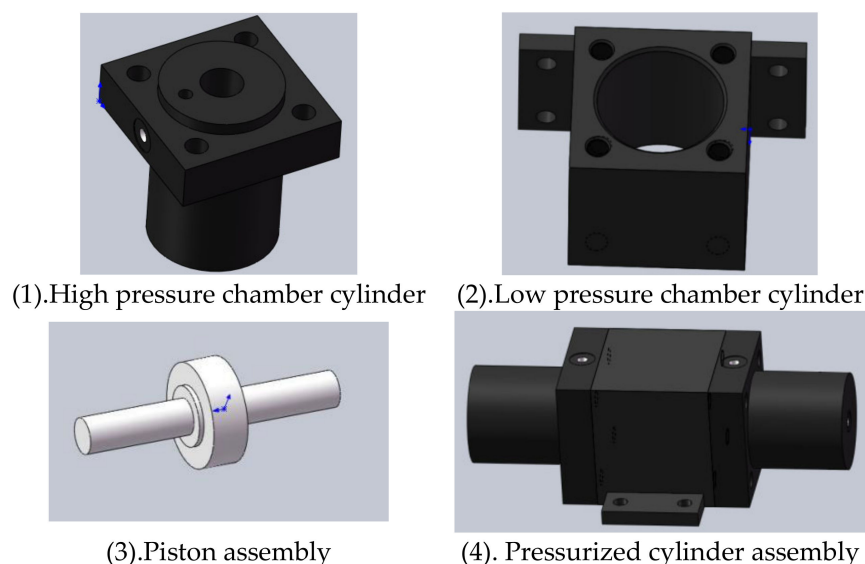### 4.2.2. Piston Rod Strength Check Calculation

The piston rod of the pressurized cylinder is compressed according to the axial direction to calculate the strength. It is obvious that as long as the piston rod of the high-pressure chamber meets the strength requirements, it will be realized. When the maximum stress is 100 MPa, which is less than 600 MPa, the safety factor is 6. Therefore, the strength of the piston rod meets the application requirements.

4.3. Finite Element Analysis of Double-Acting Liquid-Drive Pressurized Cylinder

In this paper, the finite element software ANSYS Workbench [30] is used to analyze the supercharging cylinder. Because of its wide use the ANSYS Workbench software is not introduced in detail in this article.

4.3.1. Establishment of Three-Dimensional Model of Double-Acting Pressurized Cylinder

According to the structural parameters of the pressurized cylinder calculated in the previous section, the Solidworks [31] software is used to design a three-dimensional modeling for the various components of the pressurized cylinder. Each part is physically assembly, ignoring the seal groove and the threaded hole of the oil port changed into a hole. The three-dimensional modeling of the pressurized cylinder is shown in Figure 7.

(1).High pressure chamber cylinder   (2).Low pressure chamber cylinder

(3).Piston assembly   (4). Pressurized cylinder assembly

Figure 7. 3D modeling of the pressurized cylinder.

4.3.2. Import the Created Solid Model Geometry

After the 3D model of the pressurized cylinder is established in Solidworks, it is saved as in .x_t format and then it is imported into ANSYS Workbench for the finite element analysis. Since the piston rod is moving, this paper analyzes the three working conditions of the pressurized cylinder piston, which are at the leftmost end, middle end and rightmost end. The "Face Split" tool is used to perform surface separation treatment on the pressurized cylinder which separate the pressurized portion of the pressurized cylinder chamber and the piston rod from the uncompressed portion, and use the "Symmetry" tool to symmetrically process the pressurized cylinder model. Then, a pressurized cylinder

model of three operating conditions is obtained, in which the piston is at the leftmost end as shown in Figure 8.
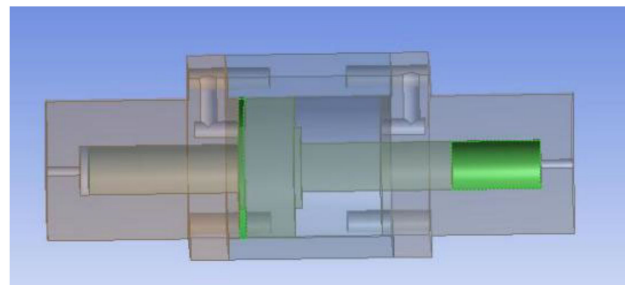

Figure 8. The piston is at the leftmost end.

4.3.3. Add Material Library to Add Model Material Properties

The material parameters are edited in "Engineering Data" and the material parameters of 45# steel are shown in Table 5.

Table 5. 45# Steel material parameters.

Parameter Name	Parameter Value
elastic modulus (GPa)	210
Poisson's ratio	0.269
Density (g/cm^3)	7.85
yield strength (MPa)	not less than 355

4.3.4. Meshing and Mesh Convergence Study

The size of the mesh directly affects the results of the calculation. The smaller the mesh size is, the higher calculation accuracy will be, but the longer the calculation time will be too. Therefore, finding an appropriate mesh size before calculation is very important which can improve the accuracy and computational efficiency of the calculation results.

Therefore, the convergence of the mesh is verified before the calculation. The model of piston rod on the right side is selected, different sizes of grids are selected, and the maximum stress is taken as the analysis index. The analysis results are shown in the Table 6. In Table 6, we find that as the number of meshes increases, the calculated index no longer changes with the increase of the mesh size, indicating that the mesh has reached convergence.

Table 6. Calculation results for different meshs.

Mesh Name	Size	Amount	Maximum Stress (MPa)
mesh-1	1	1,337,104	236.50
mesh-2	1.5	581,427	236.02
mesh-3	2	321,387	236.80
mesh-4	2.5	201,824	235.91
mesh-5	3	137,451	234.47
mesh-6	3.5	99,112	232.17
mesh-7	4	74,851	230.42
mesh-8	4.5	57,043	223.29
mesh-9	5	46,196	219.50
mesh-10	5.5	38,838	217.83

According to the above content, we adjust "Relevance" to 100, "Relevance Center" to fine, and "Element Size" to 0.002 mm. Then the number of nodes divided by the piston at the leftmost end is 944,787, and the number of cells is 586,402; the number of nodes divided at the middle end is 925,471, and the number of cells is 576,809; the number of

nodes divided at the rightmost end is 948,116, and the number of cells is 592,653. The meshing results are shown in the figure, where the piston is in the middle as shown in Figure 9.
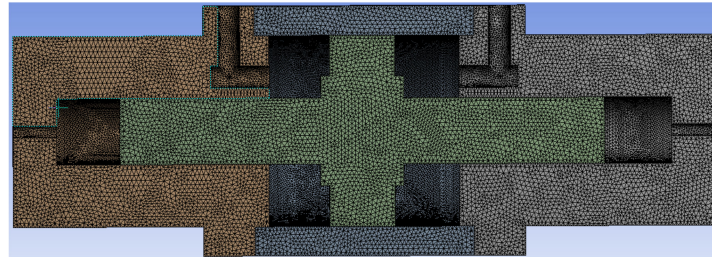

Figure 9. The piston is at the mid end.

4.3.5. Applying Loads and Constraints

The connection mode of the low pressure chamber and the high pressure chamber of the pressurized cylinder is set to "Bonded", the connection mode of the low pressure chamber and the piston is set to "Bonded", while the connection mode of the piston rod and the high pressure chamber is set to "Frictionless". The "Fixed Support" constraint is imposed on the bolt holes of the pressurized cylinder, and the "Frictionless Support" constraint is imposed on the symmetry plane of the pressurized cylinder. At the same time, a pressure of 100 MPa is applied to the high-pressure chamber of the pressurized cylinder, while a pressure of 13.7 MPa is applied to the low pressure chamber. The applied load is shown in the figure. Figure 10 shows the case where the piston is at the rightmost end, and the red part in the figure is the loading part.
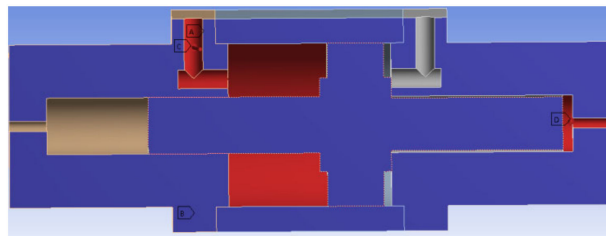

Figure 10. The piston is at the far right.

4.3.6. Post-Processing of Results

After the finite element solution, the stress analysis cloud image and the strain analysis cloud image obtained in three working conditions are respectively shown in Figures 11–13.
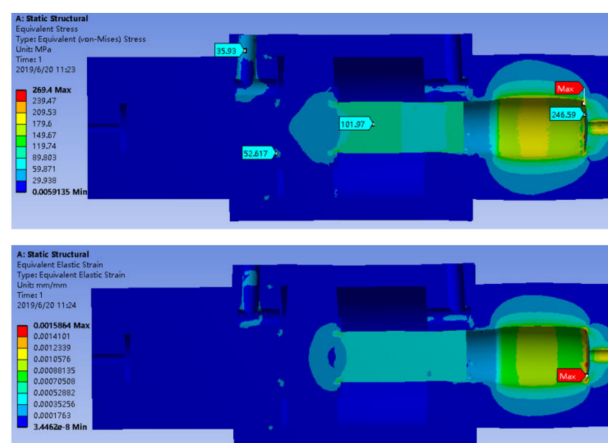

Figure 11. Stress analysis cloud and strain analysis cloud diagram when the piston is at the leftmost end.
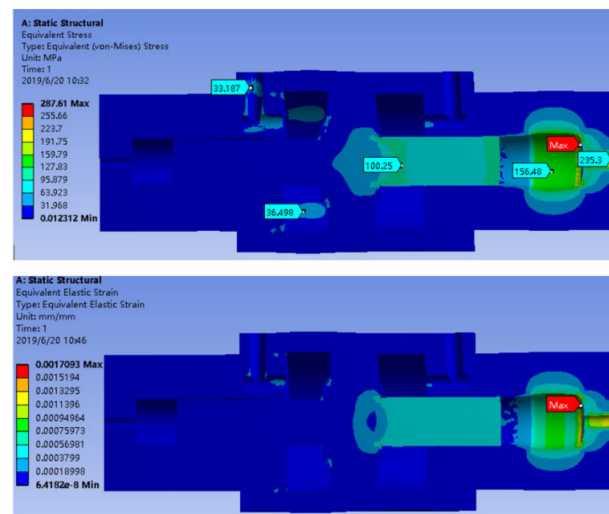
Figure 12. Stress analysis cloud and strain analysis cloud diagram when the piston is at the middle end.
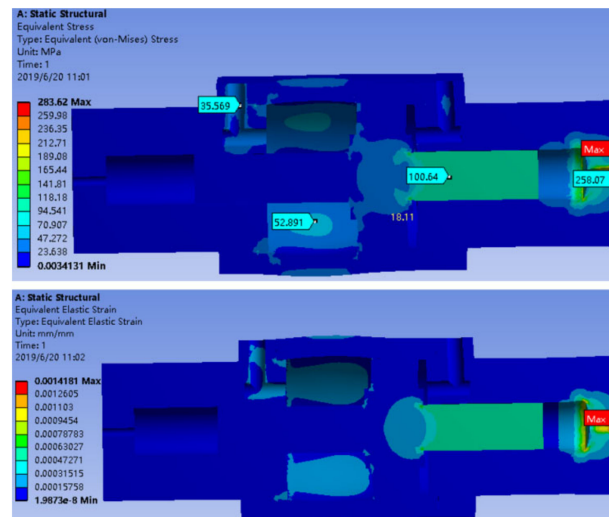

Figure 13. Stress analysis cloud and strain analysis cloud diagram when the piston is at the far right.

From the strain analysis cloud diagram of the three working conditions, it can be seen that when the piston is at the leftmost end, the strain and the deformation of the high-pressure cavity cylinder is relatively large. When the piston is at the rightmost end, the strain and the deformation of the low-pressure cavity cylinder is relatively large. When the piston is at the middle end, the strain of the high pressure and low pressure cylinders is between the front two cases.

From the stress analysis cloud diagram of the three middle working conditions, it can be seen that the maximum stress of the pressurized cylinder is concentrated at the bottom of the high-pressure chamber, and the outlet hole at the bottom of the high-pressure chamber cylinder is subjected to the the greatest stress, both of which are about 200 MPa. That is the weakest part of the pressurized cylinder. The relatively large stresses on other parts are mainly concentrated on the inner wall of the cylinder. Under the three working conditions, when the piston is in the rightmost end, the stress of the high pressure cylinder is the largest, and it is about 258.07 MPa. When the piston is at the rightmost end, the stress of the low-pressure cylinder is the largest, and it is about 52.89 MPa. The stresses received in the working conditions are basically the same, about 100 MPa.

4.4. Comparison of Theoretical Check and Finite Element Simulation Results

The simulation results of the finite element are compared with the previous theoretical calculations as shown in Table 7. In this test, the relative error E (%) is used as a measure of the accuracy of the simulation results. The calculation method is as shown in Equation (13):

$$E = \frac{\left| P_t - P_f \right|}{P_t} \times 100\% \tag{13}$$

where P_t is the theoretical calculation result, MPa; P_f is finite element simulation result, MPa.

Table 7. Comparison between simulation results and theoretical calculation results.

Method	High Pressure Cylinder Stress (MPa)	Low Pressure Cylinder Stress (MPa)	Piston Rod Stress (MPa)
finite element simulation result	258.07	52.89	101.97
theoretical calculation result	220.65	49.09	100
E (%)	16.96	7.74	1.97

From the comparison, we can see that the stress values of the finite element analysis and the theoretical calculation are basically the same. The consistency of the two methods verifies the accuracy of the calculation results and ensures the reliability of the pressurized cylinder strength. The use of finite element analysis can be more intuitive, clear and comprehensive. The results can be simulated and calculated for all parts of the pressurized cylinder.

5. Hydraulic Cylinder Performance Experimental Verification Research

5.1. Low Pressure Chamber Boost Circuit Design

This paper sets up a booster circuit in the low-pressure chamber of a double-acting pressurized cylinder. The pressure of the booster circuit is adjustable and the medium is hydraulic oil, so that they can achieve the purpose of system boosting. The low-pressure chamber portion of the pressurized cylinder is connected to the hydraulic station system. The hydraulic station system includes an oil tank, a motor, a vane pump, a pressure gauge, a pilot-operated proportional relief valve, a proportional valve electronic controller, a three-position four-way electromagnetic reversing valve, and a hydraulically controlled one-way valve. The motor and vane pump provide pressure oil for the low-pressure chamber of the pressurized cylinder. The pilot proportional relief valve and the proportional valve electronic controller ensure the stepless adjustment of the pressure in the booster circuit, thus the pressure of the high-pressure water output from the pressurized cylinder.

It can also be steplessly adjusted, and the proportional relief valve can also be used as a safety valve to ensure that the pressure oil entering the double-acting pressurized cylinder does not exceed the limit value required by the system. The three-position four-way solenoid valve ensures continuous operation of the double-acting pressurized cylinder and provides high pressure water for the test pressure. The hydraulic control check valve ensures that when the three-position four-way solenoid valve is in the neutral position, the piston of the double-acting pressurized cylinder can be fixed at any position to be stationary, so that the outlet pressure of the high-pressure chamber of the pressurized cylinder is relatively stable, starts and stops are relatively stable, the reversing position is more accurate, and the position of the reversing position is more accurate.

The two high-pressure water chambers of the double-acting pressurized cylinder are connected with a circuit composed of four check valves, so that when the pressurized cylinder piston moves to the left, the left chamber discharges high pressure water, and the right chamber suctions in water. When the piston moves to the right, the right chamber is filled with high pressure water, the left chamber suctions in water, and the water suction

and discharge process are simultaneously performed. The schematic diagram of the continuous pressurized hydraulic pressure of the hose is shown in Figure 14.
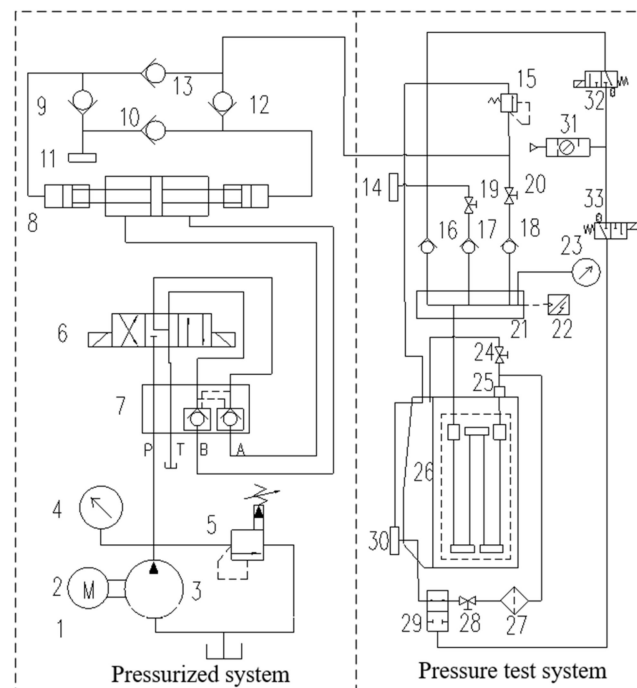

Figure 14. Booster circuit diagram. 1—tank; 2—motor; 3—vane pump; 4 and 23—pressure gauge; 5—pilot type proportional relief valve; 6—three four way solenoid valve; 7—superimposed hydraulic control check valve; 8—double acting booster cylinder; 9 and 10—water single Valve; 11—Water suction port; 12 and 13—water outlet check valve; 14—Filling port; 15—Low-pressure spillway valve; 16–18—high pressure check valve; 19,20,24 and 28—high pressure needle valve; 21—large valve block; 22—lressure transmitter; 25—small valve block; 26—experimental device; 27—high pressure filter; 29—high pressure pneumatic control valve; 30—circulating water outlet; 31—pneumatic triplex; 32 and 33—electromagnetic reversing.

5.2. Construction of the Experimental Platform

According to the actual requirements, the experimental platform is built as shown in the Figure 15, which mainly includes the test tank, the pressurized cylinder, the water tank, the hydraulic station and the control cabinet.

Figure 15. Experimental platform diagram.

5.3. Feasibility Verification Test

A 12EFG6K hose assembly was selected for pressure test. Its technical specifications require a 12EFG6K hydraulic hose to be pressurized to 100 MPa within 15 s. The length of each hose assembly was 1800 mm. To achieve the maximum hose capacity, six hose

assemblies (*V* = 3.06 L) were selected and connected using a transition joint. It is shown in Figure 16.

Figure 16. Experimental study on maximum hose capacity.

Nine groups of pressure tests were carried out on six hose assemblies, and the pressure is set to 85 MPa each time. The pressure data are recorded every second. The pressure data of the nine groups are shown in Table 8. From the standard deviation of the nine sets of data, we can see that the data measured by the experiment is stable. The pressure curve inside the hose is shown in Figure 17.

Table 8. Sheet of Pressure test data (MPa).

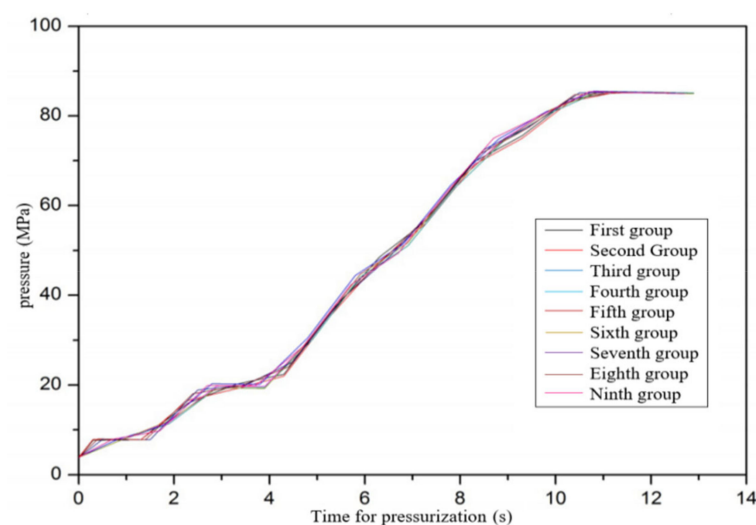| Group \ Time(s)	0 s	1 s	2 s	3 s	4 s	5 s	6 s	7 s	8 s	9 s	10 s	11 s	12 s
1	5.0	8.5	13.1	19.0	21.2	32.5	43.1	54.1	66.0	74.8	80.7	85.0	85.0
2	5.0	8.9	14.0	20.1	20.9	32.4	44.8	53.2	65.0	73.0	80.2	84.6	84.9
3	5.0	8.7	14.2	18.2	19.9	33.1	43.9	53.9	66.7	75.1	80.9	84.9	84.9
4	5.0	8.7	12.5	18.9	20.1	31.5	44.5	52.6	66.8	74.9	80.8	84.3	85.1
5	5.0	8.3	12.7	20.0	20.7	33.2	43.8	53.4	66.5	76.1	81.2	85.1	85.1
6	5.0	8.5	13.9	18.5	20.3	33.0	43.6	53.1	65.2	74.8	81.0	84.8	84.9
7	5.0	8.6	13.2	18.8	19.8	33.2	43.5	54.0	65.9	73.3	80.5	84.8	84.9
8	5.0	8.3	12.8	17.9	20.3	33.0	44.7	53.2	65.3	74.5	80.9	84.6	85.0
9	5.0	8.7	13.4	20.1	20.4	33.6	43.7	53.5	65.8	74.8	80.9	84.5	84.9
Mean value	5.0	8.6	13.3	19.1	20.4	32.8	44.0	53.4	65.9	74.6	80.8	84.7	85.0
Standard deviation	0	0.19	0.57	0.78	0.43	0.58	0.55	0.46	0.62	0.88	0.28	0.24	0.08

Figure 17. Pressure in the hose changes with pressurization time.

It can be seen from Figure 17 that the results of the nine groups of experiments show that they can be pressurized to 85 MPa within 12 s, which meets the performance requirements of the equipment. That illustrates the feasibility of the system, and verifies the rationality of the design of the pressurized cylinder. From the trend of the pressure-time curve, the time required to pressurize to 100 MPa is even about 13 s, which is shorter than the 15 s calculated by the previous design. The reason should be that the actual deformation of the hose is not theoretically analyzed. The pressure required by the pressurized system is greater and the pressurization time is shortened.

5.4. Pressure Rapidity and Stability Experiment

In order to understand the rapidity and stability of the pressurization of the pressurized cylinder, it is necessary to carry out the withstand voltage test on the hydraulic hose assembly of different hose capacities. We select the type 12EFG6K hose assembly for pressure test. Two hose assemblies (V = 1.02 L), four hose assemblies (V = 2.04 L), and six hose assemblies (V = 3.06 L) are selected and connected using a transition joint. It is shown in Figures 18–20.

Figure 18. Two hose assembly experiments.

Figure 19. Four hose assembly experiments.

Figure 20. Six hose assembly experiments.

It can be seen from Figures 21–23 that the time required for the two hose assemblies (V = 1.02 L) to be pressurized to 85 MPa is about 6.5 s, and the four hose assemblies (V = 2.04 L) are pressurized. The time required for 85 MPa is about 9 s. The time required for the six hose assemblies (V = 3.06 L) to be pressurized to 85 MPa is about 11.5 s. With the increase of the number of test hoses, the pressurization time did not increase exponentially, but increased by about 2.5 s. The reason for the analysis should be that the water from the pressurized cylinder to the hard hose of the test tool is drained after each pressure relief. When repressed, part of the flow of the pressurized cylinder is consumed. From Figures 20–22, we can see that the pressure in the hose in the first 2 s of pressurization barely increases, which confirms this point. For a maximum hose volume boost rate of 7.4 MPa/s, increasing pressure is very fast.
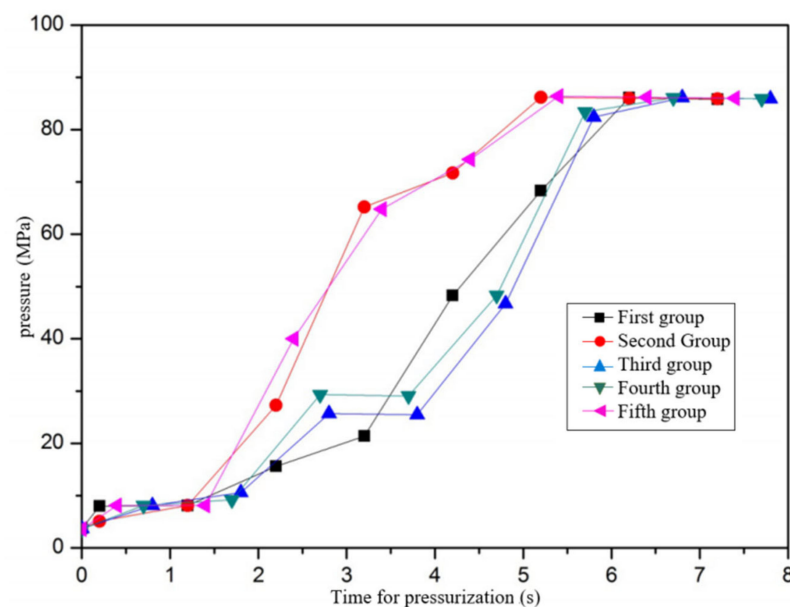

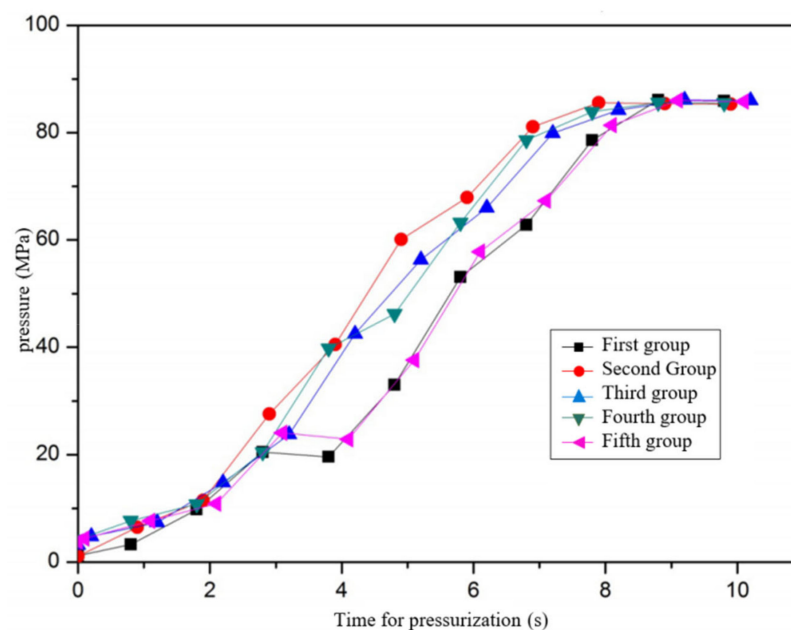**Figure 21.** Pressure time curve of two hose assemblies.

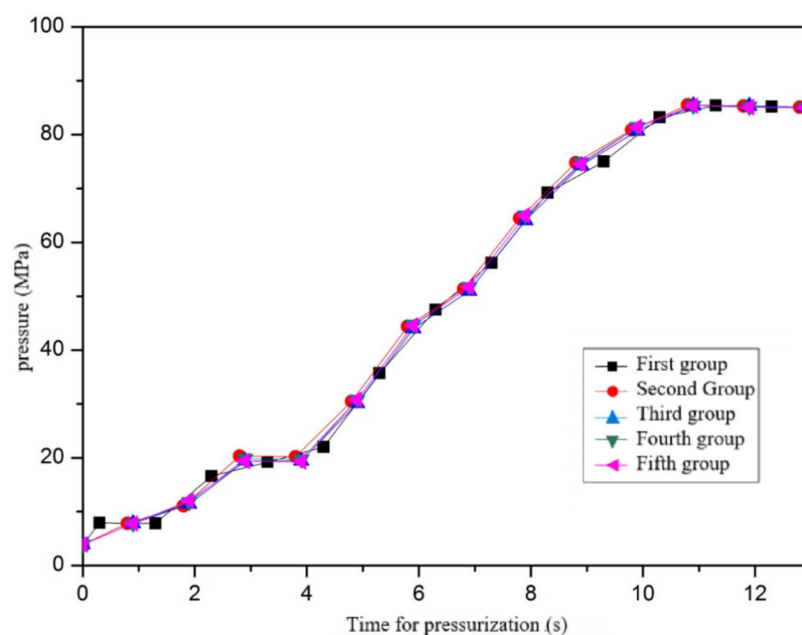**Figure 22.** Pressure time curve of four hose assemblies.

Figure 23. Pressure time curve of six hose assemblies.

From Figures 21–23, it can be seen that as the hose capacity increases, the pressure-time curve of each group of experiments becomes closer and closer, that is, the closer the time required to get pressurized to each pressure stage is, the better the pressurization stability is. The reason for the analysis should be that the hose capacity is very small, a small amount of water in the hose will cause a large pressure change, and the pressure-time curves of the experiments in each group will vary greatly.

6. Conclusions

Aiming at the problem of hydraulic hose pressure test, this paper proposes a method of continuous pressurization, which uses a double acting pressurized cylinder to provide high pressure for the pressure tests. The design calculation and strength theory check of the supercharging cylinder are carried out. Based on the finite element solution analysis of ANSYS Workbench, it is concluded that the high pressure cavity cylinder is the weak link of the pressurized cylinder. The performance of the hose pressure washer was studied experimentally, and the feasibility was verified. The pressure-pressurization time curve was obtained under the maximum hose capacity ($V = 3.06$ L). The pressure time needed to reach the maximum pressure of 85 MPa was 12 s, and the pressure rise rate was 7.4 MPa/s. This paper also studies the pressure-holding performance and provides a quantitative basis for judging whether the pressure test of rubber hose is successful or not. It is concluded that the larger the hose capacity is, the better the pressure stability is.

Due to the limitations of the production line and the objective conditions of the equipment, there are still many problems to be studied: in this paper, there is no built-in sensor designed for the pressurized cylinder to monitor the piston position and buffer structure, which will make the piston rod impact. Therefore, further dynamic analysis of the pressurized cylinder can be carried out.

Author Contributions: Conceptualization, C.Z.; methodology, X.N., G.H., C.Z. and L.L.; validation, X.N. and G.H.; formal analysis, X.N. and G.H.; writing—original draft preparation, X.N.; writing—review and editing, C.Z.; supervision, C.Z. and L.L.; project administration, L.L.; funding acquisition, C.Z. All authors have read and agreed to the published version of the manuscript.

Institutional Review Board Statement: Not applicable.

Informed Consent Statement: Not applicable.

Data Availability Statement: The data used in this study is self-test and self-collection. Data cannot be shared at present.

Nomenclature

P_1: the input pressure of the low pressure chamber; P_2, the output pressure of the high pressure chamber; d, the inner diameter of the low pressure chamber; D, the inner diameter of the high pressure chamber; d_1, the diameter of the test hose assembly; L_1, the total length of the test hose assembly; V_1, the maximum volume; P, the pressure after water is pressurized; P_0, the pressure of pre-flush before water is pressurized; β_w , water's compression coefficient; d_n, the diameter of the hose when subjected to a pressure of 100 MPa; d_0, the diameter of the hose when subjected to a pressure of 10 MPa; L, the total length of the hose when subjected to a pressure of 100 MPa; L_0, the total length of the hose when subjected to a pressure of 10 MPa; L_z, the total stroke; L_r, the single stroke; σ_r, radial compressive stress; σ_θ, tangential tensile stress; σ_s, axial tensile stress; P, test pressure; R_0, the outer wall radius of the cylinder; R_i, the radius of the inner wall of the cylinder; r, free radius of the cylinder; K, the ratio of R_0 to R_i; n_G, safety factor; P_t, the theoretical calculation result; P_f, finite element simulation result.

References

1. Tsuda, K.; Umeda, K.; Kota, I.; Sakaino, S.; Tsuji, T. Analysis on rigidity of hydraulic hoses for electro-hydrostatic actuators. In Proceedings of the IECON 2017—43rd Annual Conference of the IEEE Industrial Electronics Society, Beijing, China, 29 October–1 November 2017; pp. 2828–2833.
2. Fedorko, G.; Molnar, V.; Dovica, M.; Toth, T.; Fabianová, J. Failure analysis of irreversible changes in the construction of the damaged rubber hoses. *Eng. Fail. Anal.* **2015**, *58*, 31–43. [CrossRef]
3. Wang, X.K.; Xi, S.H.; Chen, Y. A dangerous type of failure mode of aircraft PTFE hose assembly and reliability measures. In Proceedings of the 2012 International Conference on Quality, Reliability, Risk, Maintenance, and Safety Engineering, Chengdu, China, 15–18 June 2012; pp. 1309–1313.
4. Tonatto, M.L.P.; Tita, V.; Araujo, R.T.; Forte, M.M.C.; Amico, S.C. Parametric analysis of an offloading hose under internal pressure via computational modeling. *Mar. Struct.* **2017**, *51*, 174–187. [CrossRef]
5. Sampath, K.H.S.M.; Perera, M.S.A.; Ranjith, P.G. Theoretical overview of hydraulic fracturing break-down pressure. *J. Nat. Gas. Sci. Eng.* **2018**, *58*, 251–265. [CrossRef]
6. Kwak, S.B.; Choi, N.S. Micro-damage formation of a rubber hose assembly for automotive hydraulic brakes under a durability test. *Eng. Fail. Anal.* **2009**, *16*, 1262–1269. [CrossRef]
7. Yang, Z.J.; Chen, D.Y.; Zhou, L.Q.; Gao, Y. Study on stress distribution of multilayer steel wire wound hose under the condition of oil pressure. In Proceedings of the 2016 12th IEEE/ASME International Conference on Mechatronic and Embedded Systems and Applications (MESA), Auckland, New Zealand, 29–31 August 2016; pp. 1–6.
8. Li, W.D. Design and application of fast gas-liquid pressurized cylinder in Chinese. *Mach. Tool Hydraul.* **2004**, *2*, 102–103.
9. Ding, H.G.; Zhao, J.Y.; Zhu, Q.M. A New Hydraulic Speed Regulation Scheme: Valve-Pump Parallel Variable Mode Control. *IEEE Access.* **2018**, *6*, 55257–55263. [CrossRef]
10. Cho, N.-C.; Hwang, I.-J.; Lee, C.-M.; Park, J.-W. An experimental study on the airlift pump with air jet nozzle and booster pump. *J. Environ. Sci. Suppl.* **2009**, *21*, 19–23. [CrossRef]
11. Chen, J.; Zio, E.; Li, J.; Zeng, Z.; Bu, C. Accelerated life test for reliability evaluation of pneumatic cylinders. *IEEE Access.* **2018**, *6*, 75062–75075. [CrossRef]
12. Seo, S.; Han, S.; Lee, S.; Chang, D. A pump-free boosting system and its application to liquefied natural gas supply for large ships. *Energy* **2016**, *105*, 70–79. [CrossRef]
13. Fu, C.A.; Zhang, X.Y. Discussion on ultra-high pressure hydraulic technology in Chinese. *Hydr. Pneu. Seals.* **2010**, *30*, 4–6.
14. Wang, J.G. Current status and development trend of ultra-high pressure hydraulic technology at home and abroad in Chinese. *China Heavy Equipment.* **2013**, *2*, 6–7.

15.　Gong, Q.H.; Bu, Y.; Wang, X.D. Research on ultra-high pressure technology of hydraulic system in Chinese. *Coast. Enter. Tech.* **2007**, *1*, 81–83.

16.　Wang, X.X. Introducing a novel gas-liquid supercharging system in Chinese. *Chin. Hydr. Pneu.* **2002**, *11*, 43–45.

17.　Navatha, A.; Bellad, K.; Hiremath, S.S.; Karunanidhi, S. Dynamic analysis of electro hydrostatic actuation System. *Procedia Technol.* **2016**, *25*, 1289–1296. [CrossRef]

18.　Diaz, C.; Ruiz, F.; Patino, D. Modeling and control of water booster pressure systems as flexible loadsfor demand response. *Appl. Energy* **2017**, *204*, 106–116. [CrossRef]

19.　Zhao, S.D.; Meng, D.A.; Li, J.X.; Fan, S.Q.; Li, X.; Chen, C. A double-acting servo booster cylinder for press. China Patent CN103939427A, 23 July 2014.

20.　Jiao, N.; Guo, J.J.; Liu, S.L. Hydro-pneumatic suspension system hybrid reliability modeling considering the temperature influence. *IEEE Access* **2017**, *5*, 19144–19153. [CrossRef]

21.　Shao, Y.Q.; Liu, J.S.; Zhou, S.J. Application of double-acting reciprocating supercharger on six-sided top press in Chinese. *Sup. Mat. Eng.* **2013**, *25*, 31–33.

22.　Liu, J.X. Finite element analysis and simulation of steel wire wrapped hose skeleton structure. Master's Thesis, Qingdao University of Science and Technology, Qingdao, China, 2013.

23.　Xie, Y.B. Development and Test Method of Small Ultra-high Pressure Sealing Test Device in Chinese. *Hydr. Pneu. Seals.* **2013**, *4*, 37–40.

24.　Wang, B.; Zhang, N.; Ji, H.Y. Study on precise displacement control of a miniature hydraulic system via RBF-DOB. *IEEE Access* **2018**, *6*, 69162–69171. [CrossRef]

25.　Zhang, Y.J. Discussion on selection and maintenance of ultra high pressure seal of automatic high pressure water test machine in Chinese. *Fluid Power Tran. Contr.* **2008**, *1*, 57–59.

26.　Yan, W.Q. A new type of paste-type high pressure ultra high pressure seal and its application in Chinese. *Min. Res. Dev.* **2009**, *29*, 57–58.

27.　Liu, D.X. Selection of ultra high pressure hydraulic cylinder seals in Chinese. *Mech. Eng.* **2009**, *9*, 128–129.

28.　Zhao, W.H. Principle design and application of fast gas-liquid pressurized cylinder in Chinese. *Mac. Des. Man. Eng.* **2009**, *38*, 62–64.

29.　Liu, H.W. *Mechanics of Materials*; Higher Education Press: Beijing, China, 2011.

30.　Huang, Z.X.; Liu, C.Z. *Manual Book for ANSYS Workbench 14.0*; Posts and Telecom Press: Beijing, China, 2013.

31.　Zhao, F.; Yang, X.J.; Zhao, N. *SolidWorks 2016 Chinese Version of Mechanical Design from Entry to the Master*; Posts and Telecom Press: Beijing, China, 2016.